Experimental determination of L fluorescence yields of gadolinium

Yves Ménesguen, Marie-Christine Lépy

▶ **To cite this version:**

Yves Ménesguen, Marie-Christine Lépy. Experimental determination of L fluorescence yields of gadolinium. X-Ray Spectrometry, 2020, 49 (5), pp.596-602. 10.1002/xrs.3157 . hal-04548331

HAL Id: hal-04548331
https://hal.science/hal-04548331

Submitted on 16 Apr 2024

HAL is a multi-disciplinary open access archive for the deposit and dissemination of scientific research documents, whether they are published or not. The documents may come from teaching and research institutions in France or abroad, or from public or private research centers.

L'archive ouverte pluridisciplinaire **HAL**, est destinée au dépôt et à la diffusion de documents scientifiques de niveau recherche, publiés ou non, émanant des établissements d'enseignement et de recherche français ou étrangers, des laboratoires publics ou privés.

Experimental determination of L fluorescence yields of gadolinium

Y. Ménesguen[1], M.-C. Lépy[1]

[1]CEA, LIST, Laboratoire National Henri Becquerel (LNE-LNHB), bât 602 PC 111, CEA-Saclay, 91191 Gif-sur-Yvette , France

Abstract

The fluorescence yields are useful x-ray atomic fundamental parameters for x-ray spectrometric purposes but suffer from large tabulated uncertainties, and this is the first time to our knowledge that all three subshell parameters are measured together. We determined the three L partial fluorescence yields and the associated Coster-Kronig transition probabilities of gadolinium, by selectively ionizing the three L subshells with a tunable monochromatic photon beam. We found $\omega_1 = 0.099(3)$, $\omega_2 = 0.162(4)$ and $\omega_3 = 0.159(3)$ that are in good agreement with tabulated values, but our derived uncertainties are significantly reduced.

keywords: fluorescence yields, gadolinium, mass attenuation coefficients

1 Introduction

X-ray atomic parameters such as mass attenuation coefficients, diagram line energies, fluorescence yields are required in large variety of applications that rely on x-ray based techniques. These parameters quantify the interaction of photons with matter, what is necessary to model the physics of technique. After a large amount of experimental or theoretical studies in the sixties and seventies, the interest of the community in performing new measurements decreased. For example, the number of papers dealing with mass attenuation measurements collapsed in the nineties [1]. While some elements attracted a lot of work regarding one fundamental paramental or the other, the available x-ray database and compilations can rely on several publications, in some other cases, very few publications if none are available and databases must rely on theoretical calculations or extrapolated/interpolated values [2, 3, 4, 5]. Most of the time, uncertainties are not quoted, which makes it questionable to pretend having reliable results using them. To overcome these drawbacks, an international effort is being undertaken to improve the reliability of the x-ray fundamental parameters of elements.

In our recent work about the L and M diagram line energies of gadolinium [6], we started by measuring the mass attenuation coefficients and their associated uncertainties over a wide range of photon energies including N, M and L absorption edges. This allowed us to identify weak M lines by checking the consistency of two experimental approaches having different calibration procedures. Following this first step of line identification, the line absolute intensities are the other parameters important to qantify. In the present paper, we focussed our work on the partial L fluorescence yields and made our experimental investigations with an energy-dispersive spectrometer, thus leading to poorer spectral resolution than a double-crystal spectrometer but making it possible to calibrate its energy-dependent efficiency [7].

In the case of the fluorescence yields, very few experimental works are published and among them also some incomplete sets of values. Therefore, available tables provide interpolated values. Two sources published theoretical values of the partial L fluorescence yields [8, 9], and two other are compilations that rely on interpolation on fitting curves from nearest elements [10, 11]. The xraylib library is also providing values [12] for the L partial fluorescence yields but they are derived from already cited works. In general, there are not so many different sources of experimental values for high-Z elements and that is a reason for being mistrustful in proposed values and their associated uncertainties if any.

2 Experimental conditions

The experimental fluorescence spectra were acquired at the SOLEIL synchrotron (France) on the hard X-rays branch of the metrology beamline to get monochromatic X-rays in the 3-30 keV energy range. Its double Si(111) cristal monochromator was aligned as described in [13] to minimize harmonics and stray light, and the Bragg angle was calibrated with respect to K-absorption edges of pure metal foils as detailed in [6], its energy resolution is measured as $\Delta E/E \leq 1.7 \times 10^{-4}$ at the copper K absorption energy edge. We used a sample of 10 µm of nominal thickness to measure the L fluorescence lines. This thin foil was used in [6] and its mass per unit area is known with an excellent accuracy (less than 1% typically) as well as its purity. It was weighted 10.664(10) mg with an area of 135.52(10) mm^2.

The x-ray fluorescence of the sample was studied using an experimental setup where the energy-dispersive spectrometer (SDD) is set at 90° from the incident beam and the sample is at 45° from both the incident beam and the spectrometer directions. The SDD has an energy resolution of 128 eV at 5.9 keV. The incident photon beam energy was chosen to ionize sequentially the three L subshells.

3 Partial L fluorescence yields

3.1 The fluorescence cross-sections

The emitted x-ray fluorescence, originated by photoionization, is the result of several processes that include the attenuation of the incoming and emitted fluorescence photons in the target, the photoelectric effect and atomic relaxation including subshell rearrangements. Without any vacancy exchange between subshells, the general formula linking the number of counts in the full-energy peak of a specific x-ray line to the intensity of the incoming photon beam is the Sherman's equation for a pure element [14]:

$$\frac{I_i}{\eta_i} = \int_0^1 I_0 \times \frac{\Omega}{4\pi} \times \omega_i \times \tau_0 \times \frac{M}{A} \times \exp\left(-\mu_0 \times \frac{M}{A} \times \frac{x}{\sin(\beta)}\right) \times \exp\left(-\mu_i \times \frac{M}{A} \times \frac{x}{\sin(\theta)}\right) \times \frac{dx}{\sin(\beta)} \qquad (1)$$

where I_0 is the number of photons per unit time of the incoming beam with energy E_0 and I_i is the full-energy peak area for characteristic x-rays with energy E_i, η_i is the detection efficiency at photon energy E_i, Ω is the solid angle of detection, ω_i is the partial fluorescence yield of the diagram line of interest, τ_0 is the partial photoelectric coefficient at photon energy E_0, M and A are respectively the mass (in g) and area (in cm^2) of the sample, β is the incidence angle and θ the detection angle, both being 45°. The detection efficiency η_i was experimentally determined by comparison with a reference detector on the lab-source SOLEX as in [7]. μ_0 and μ_i are the total mass attenuation coefficients at the excitation energy E_0 and at the characteristic energy E_i, respectively. As several lines originates from a single subshell, we summed the fluorescence production cross sections of diagram lines belonging to the same subshell (Table 2). In equation (1), the parameters M, A, $\mu_{0,i}$, Ω, $I_{0,i}$ and η_i are independently measured, leaving the partial fluorescence yields ω_i and the photoelectric cross sections τ_0 as the two unknowns of the equation. The integration of equation (1) gives the fluorescence production cross section σ_i:

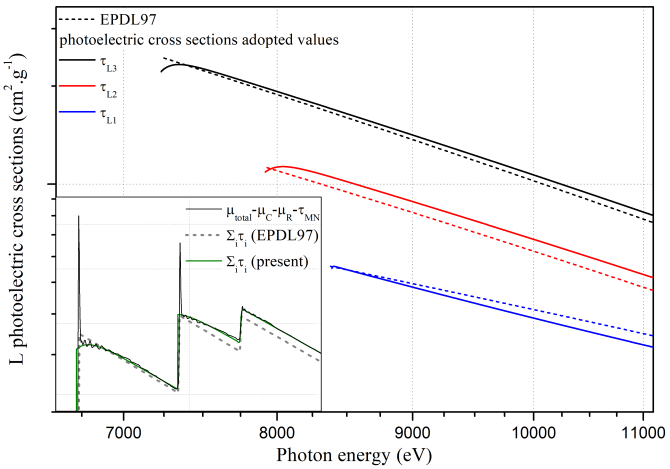

Figure 1: Partial L photoelectric cross-sections from EPDL and adopted values. Insert : μ_C and μ_R are the Compton and Rayleigh scattering respectively.

$$\omega_i \times \tau_0 = \sum_j \frac{\frac{I_j}{\eta_j}}{I_0 \times \frac{\Omega}{4\pi} \times \frac{1-\exp\left(-(\mu_0+\mu_j)\times\frac{M}{A}\times\sqrt{2}\right)}{(\mu_0+\mu_j)}} = \sigma_i \tag{2}$$

where the fluorescence intensities values I_j with indices j correspond to the diagram lines with inner-shell origin L_i.

This expression is valid for K-fluorescence yields but must be slightly modified for L-lines in order to take into account the Coster-Kronig effect. Coster-Kronig transitions happen between subshells with the same principal quantum number, making it possible for a primary vacancy created in one of the subshells to shift to a higher subshell before the initial vacancy is filled by another transition [4]. The Coster-Kronig transition probabilities are represented by the f_{ij} parameters and modify equation (2). Indeed, in the case of a diagram line starting from a vacancy in the L_3 subshell, τ_0 becomes $\tau_{3,0}$ for incoming photons with an energy E_0 between the L_3 and L_2 absorption edges. For energies larger than the L_2 absorption edge, vacancy transfers from one subshell to another are taken into account by the Coster-Kronig transition probabilities f_{kl} from subshell k to subshell l. Thus, depending on which subshell the primary vacancy is created as well as on the diagram line considered, the fluorescence production cross sections values σ are summed up in Table 1 for the L subshells.

Table 1: Equations of the L fluorescence production cross sections and L absorption edges energies (in eV).

$E_{L_3} = 7246.6(28)$	$E_{L_3} \leq E_0 \leq E_{L_2}$	$\sigma_3 = \omega_3 \times \tau_{3,0}$
$E_{L_2} = 7930.0(30)$	$E_{L_2} \leq E_0 \leq E_{L_1}$	$\sigma_3 = \omega_3 \times (\tau_{3,0} + f_{23} \times \tau_{2,0})$ $\sigma_2 = \omega_2 \times \tau_{2,0}$
$E_{L_1} = 8377.3(10)$	$E_{L_1} \leq E_0$	$\sigma_3 = \omega_3 \times (\tau_{3,0} + f_{23} \times \tau_{2,0} + (f_{13} + f_{12} \times f_{23}) \times \tau_{1,0})$ $\sigma_2 = \omega_2 \times (\tau_{2,0} + f_{12} \times \tau_{1,0})$ $\sigma_1 = \omega_1 \times \tau_{1,0}$

3.2 Photoelectric cross-sections

The partial photoelectric cross sections mentioned in equation 2 cannot be measured experimentally independently from the fluorescence yields. Thus, we evaluate them from the experimental mass atten-

uation coefficients already determined in [6] and we use the theoretical values from the EPDL97 [15] as initial guess. In Figure 1 (insert), the black line represent the total L photoelectric cross sections calculated as $\mu - \mu_{Compton} - \mu_{Rayleigh} - \tau_{MN}$ where $\mu_{Compton}$ and $\mu_{Rayleigh}$ are respectively the incoherent and coherent cross sections taken from EPDL97 and τ_{MN} represents the photoelectric cross sections of the M and N shells calculated as an extrapolation of the total mass attenuation coefficients curve from energies smaller than $E_{L_3}$for energies larger than the L absorption edges.

The partial photoelectric cross sections $\tau_{L3,2,1}$, in equation 1, were adjusted with two criteria. First, their sum must match $\mu - \mu_{Compton} - \mu_{Rayleigh} - \tau_{MN}$, illustrated by the superposition of the black and green curves in the insert of Figure 1. The second criterion used the derived values of the partial fluorescence yields. In energy ranges where no Coster-Kronig effects are involved in the emission of photons, the energy dependence of the fluorescence cross sections σ_i is only due to the photoelectric cross sections. For example, for excitation energies E_0 larger than the L_3 absorption edge and lower than the L_2 edge, the emitted photons are due to the filling of vacancies in the L_3 subshell thus the derived fluorescence cross section σ_3 is the product $\omega_3 \times \tau_{3,0}$ where ω_3 is the partial L_3 fluorescence yields and $\tau_{3,0}$ is the photoelectric cross section due to subshell L_3 at excitation energy E_0. The fluorescence yields remaining constant, it allows to derive the energy-dependence of the photoelectric cross sections τ_3. The same procedure applies for other subshells and the derived photoelectric cross sections that fulfill these two constraints are presented in Figure 1. While the energy-dependence between our adopted values and those from EPDL97 are rather similar, it seems that our values for τ_2 are significantly larger in all cases.

4 Results of the partial L fluorescence yields

4.1 Spectra acquisitions and peaks identification

Thirty spectra are acquired at increasing excitation energies from 7.3 to 15 keV to allow to identify the contributions from the three L subshells. We identified fifteen diagram lines in the acquired spectra, that were fitted with our COLEGRAM software [16] using Voigt functions. The line energies and natural widths were taken from [6, 17]. The background of all spectra were processed to take into account the dicontinuity due to the presence of a peak. Some of these lines could not be distinguished as they are too close. The diagram line $L\alpha_1$ includes $L\alpha_2$ and $L\eta$ for energies larger than the L_2 absorption edge. For the same reason, $L\beta_1$ and $L\beta_4$, $L\beta_3$ and $L\beta_6$, $L\beta_2$ and $L\beta_{15}$, $L\beta_7$ and $L\beta_5$, $L\gamma_6$ and $L\gamma_8$ are identified as a single line. All the diagram lines are presented in Table 2.

Table 2: Diagram lines (transition and energies). Transitions in blue are detected together with a more intense line.

Line	Transition	Energy (eV)	Line	Transition	Energy (eV)	Line	Transition	Energy (eV)
Ll	L_3M_1	5362.6(30)	$L\beta_1$	L_2M_4	6713.42(13)	$L\gamma_5$	L_2N_1	7547(3)
Lt	L_3M_2	5559.7(28)	$L\beta_4$	L_1M_2	*6686.67(11)*	$L\gamma_1$	L_2N_4	7787(3)
Ls	L_3M_3	5703.1(28)	$L\beta_6$	L_3N_1	6865.25(23)	$L\gamma_6$	L_2O_4	7912(3)
$L\alpha_1$	L_3M_5	6056.8(3)	$L\beta_3$	L_1M_3	*6831.50(16)*	$L\gamma_8$	L_2O_1	*7899.5(30)*
$L\alpha_2$	L_3M_4	*6024.5(3)*	$L\beta_2$	L_3N_5	7102.38(18)	$L\gamma_2$	L_1N_2	8085.3(14)
$L\eta$	L_2M_1	*6048.3(3)*	$L\beta_{15}$	L_3N_4	*7098.2(7)*	$L\gamma_3$	L_1N_3	8124.3(14)
$L\beta_{17}$	L_2M_3	6394.3(30)	$L\beta_7$	L_3O_1	7220(3)	$L\gamma_4$	L_1O_4	8360.8(14)
			$L\beta_5$	$L_3O_{4,5}$	*7238.6(30)*			

Figure 2 presents the Ll, Lt, Ls, $L\alpha_{1,2}$, $L\beta_6$, $L\beta_{2,15}$ and $L\beta_{7,5}$ lines from the L_3 subshell. An averaged ratio of the $L\beta_6/L\alpha_{1,2}$ lines intensities is obtained and is used as input for spectra taken at excitation energies larger than the L_2 absorption edge because $L\beta_6$ cannot be further distinguished from $L\beta_1$, limited by the detector resolving power. The lines $L\eta$, $L\beta_{17}$, $L\beta_1$, $L\gamma_5$, $L\gamma_1$, $L\gamma_{6,8}$ arise when exciting

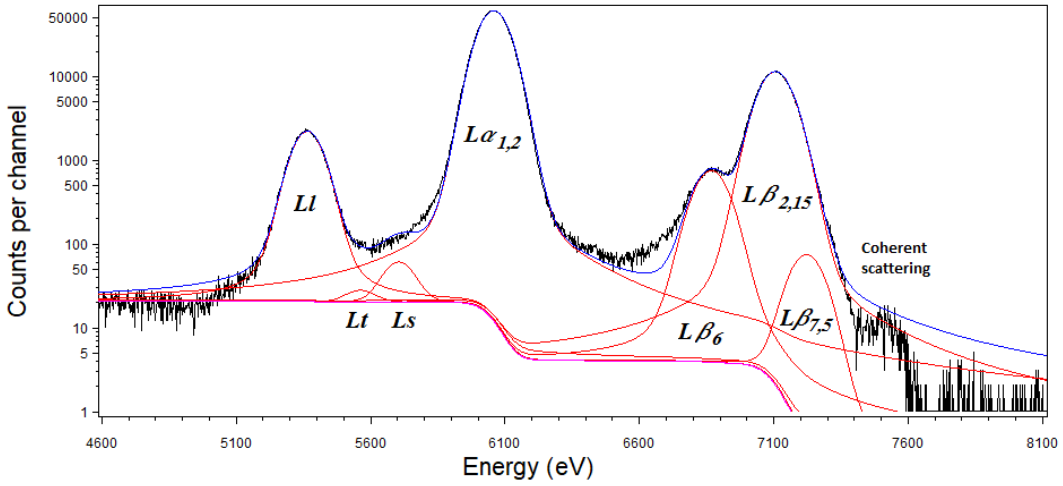

Figure 2: Gadolinium L lines for excitation energy $E_{L_3} \leq E_0 \leq E_{L_2}$.

with photons of energies larger than E_{L_2}, as presented in Figure 3. Unfortunately, $L\eta$ cannot be distinguished from $L\alpha_{1,2}$ and its contribution was subtracted by taking its intensity equal to 0.027*$L\beta_1$ [18]. Finally, at excitation energies larger than E_{L_1}, the lines $L\beta_3$, $L\beta_4$, $L\gamma_2$, $L\gamma_3$ and $L\gamma_4$ are showing up (Fig. 4). Once again, some of these new lines cannot be separated and their contribution must subtracted using the experimental ratios as measured in [6]. The diagram line $L\beta_4$ is hidden by $L\beta_1$and $L\beta_3$ by $L\beta_6$ ($L\beta_6$ already evaluated as a fixed ratio of the $L\alpha_{1,2}$ line). The contribution of $L\beta_4$ is subtracted from the $L\beta_1$ line intensity by taking its intensity equal to 0.56*$L\beta_3$ [6].

4.2 Results and assessment of uncertainties

We summed all lines from the same subshell in order to get the total subshell fluorescence yields. We averaged the derived partial L-fluorescence yields obtained with the spectra taken at different excitation energies among the same subshell and present our results in Table 4. From equation 2, we derived the following individual contributions to the final uncertainties according to the GUM [19]:

$$\left(\frac{d\omega_i}{\omega_i}\right)^2 \approx \left(\frac{dI_j}{I_j}\right)^2 + \left(\frac{dI_0}{I_0}\right)^2 + \left(\frac{d\Omega}{\Omega}\right)^2 + \left(\frac{dM}{M}\right)^2 + \left(\frac{dA}{A}\right)^2 + \left(\frac{d\tau_{i,0}}{\tau_{i,0}}\right)^2 + \left(\frac{A}{2\sqrt{2}M\mu_0}\right)^2 \times \left(\left(\frac{d\mu_0}{\mu_0}\right)^2 + \sum_j \left(\frac{d\mu_j}{\mu_j}\right)^2\right) \quad (3)$$

The first two terms accounts for the statistics and are taken as the standard deviations resulting from the global fitting of all fluorescence cross sections. The contributions from the mass attenuation coefficients is energy-dependent and always kept under 0.25%. The different contributions are listed in Table 3, they are determined either by direct experimental estimate (mass, area, solid angle, counting statistics, mass attenuation coefficients) or indirectly (photoelectric cross sections). The dominant terms are due to the statistics and is around 3% for the three partial fluorescence yields.

Table 3: Relative standard uncertainties contributing to the total uncertainty.

Origin	Mass	Area	Solid angle	Counting statistics	Photoelectric cross sections	Mass attenuation coefficients
Contribution (%)	0.1	0.08	1	<3	<0.5	<0.25

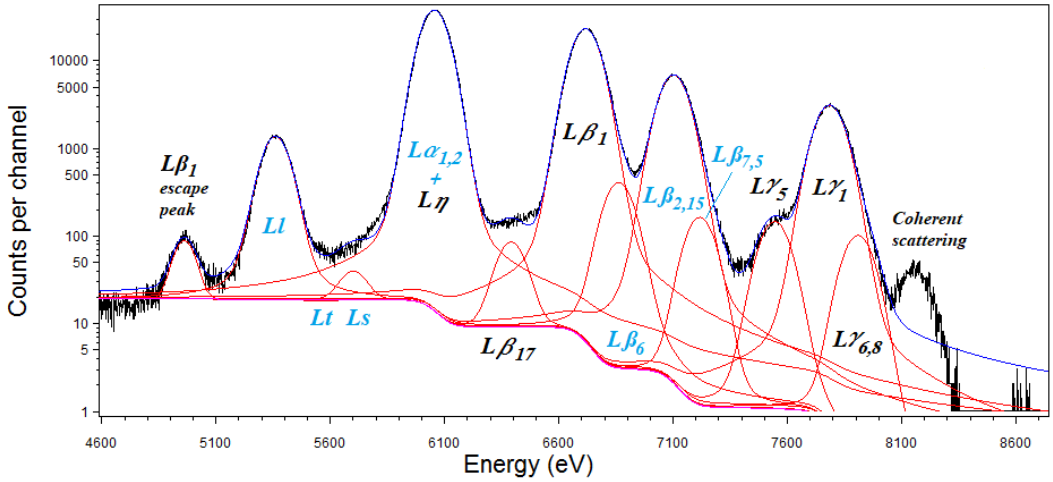

Figure 3: Gadolinium L lines for excitation energy $E_{L_2} \leq E_0 \leq E_{L_1}$.

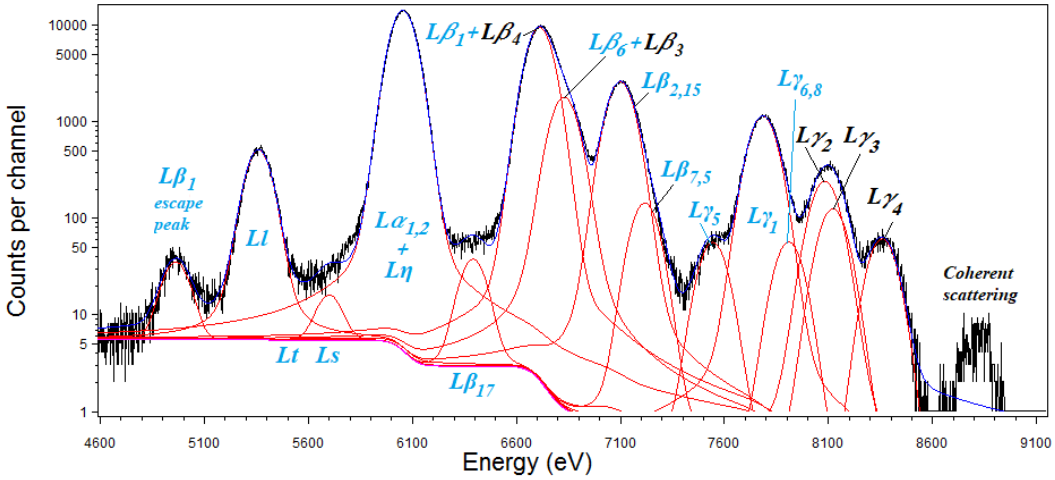

Figure 4: Gadolinium L lines for excitation energy $E_{L_1} \leq E_0$.

In the past, the average L-fluorescence yields was more commonly used as it was easier to measure when spectrometers had poor resolution. The average L-fluorescence yields is a combination of the partial fluorescence yields, the Coster-Kronig transition probabilities and the partial photoelectric cross-sections as explained in [3, 10]. In spite of being obsolete nowadays, this is the only way to compare with ancient experimental values reported in [3] such as [20]. The most recent work from Papp et al. [21] reports only on the ω_1, f_{12} and f_{13}. For most comparison, we found a good agreement for the partial fluorescence yields but significant discrepancies for the Coster-Kronig factors especially for f_{12}. Indeed our measurements did not show a significant contribution of the photoionisation of the L_1 subshell in the fluorescence lines of responsibles for ω_2.

5 Conclusion

To our knowledge, this is the first experimental measurement of the three L partial fluorescence yields of gadolinium. Nevertheless, we found a good agreement with tabulated values for $\omega_{1,2,3}$ despite the

Table 4: Partial L-fluorescence yields and Coster-Kronig transition probabilities. The "Origin" column stands for experimental (exp), theoretical (th) and compilation (comp).

	Origin	$\bar{\omega_L}$	ω_1	ω_2	ω_3	f_{12}	f_{13}	f_{23}
Present	exp	0.163(1)	0.099(3)	0.162(4)	0.159(3)	0.053(23)	0.27(4)	0.095(20)
Singh [20]	exp	0.184(5)						
Papp [21]	exp		0.101(5)			0.166(20)	0.287(14)	
Perkins [8]	th		0.0765	0.174	0.164			
Puri [9]	th		0.083	0.175	0.167	0.216	0.334	0.160
Krause [10]	comp		0.079(12)	0.158(11)	0.155(8)	0.19(3)	0.30(3)	0.147(25)
Campbell [11]	comp		0.09	0.175	0.167	0.19	0.25	0.15
xraylib [12]	comp		0.102	0.158	0.155	0.19	0.279	0.149

scattering of the scarce published values. On the contrary, our experimental Coster-Kronig transition probabilities are significantly different from those in tables but these values are questionable as no experimental work was never done and they rely only on theoretical calculations or extrapolations in compilations. The derived values of the Coster-Kronig transition probabilities are strongly dependent of the fluorescence yields as well as the photoelectric cross sections explaining why we still have some discrepancies and rather large associated uncertainties, especially for f_{12}. Nevertheless, we have an excellent agreement for ω_1 and f_{13} with the most recent experimental values from Papp [21].

6 Acknowledgments

Y. Ménesguen, M.-C. Lépy acknowledge the financial support for the measurements of a part of the data by the REXDAB Collaboration that was initiated within the International Fundamental Parameter Initiative.

References

[1] Y. Ménesguen, C. Dulieu, and M.-C. Lépy, "Advances in the measurements of the mass attenuation coefficients," *X-ray Spectrometry*, pp. 1–6, 2018.

[2] B. L. Henke, E. M. Gullikson, and J. C. Davis, "X-ray interactions: photoabsorption, scattering, transmission, and reflection at E = 50-30000 eV, Z = 1-92," *Atomic Data and Nuclear Data Tables*, vol. 54, no. 2, pp. 181–342, 1993.

[3] J. H. Hubbell, P. N. Trehan, N. Singh, B. Chand, D. Mehta, M. L. Garg, R. R. Garg, S. Singh, and S. Puri, "A Review, Bibliography, and Tabulation of K, L, and Higher Atomic Shell X-Ray Fluorescence Yields," *Journal of Physical and Chemical Reference Data*, vol. 23, no. 2, pp. 339–364, 1994.

[4] W. Bambynek, B. Crasemann, R. W. Fink, H.-U. Freund, H. Mark, C. D. Swift, R. E. Price, and P. Venugopala Rao, "X-ray fluorescence yields, Auger, and Coster-Kronig transition probabilities," *Reviews of Modern Physics*, vol. 44, no. 4, pp. 716–813, October 1972.

[5] G. Zschornack, *Handbook of X-ray Data*. Springer-Verlag, 2007.

[6] Y. Ménesguen, M.-C. Lépy, Y. Ito, M. Yamashita, S. Fukushima, M. Polasik, K. Słabkowska, L. Syrocki, E. Węder, P. Indelicato, J. Marques, J. Sampaio, M. Guerra, F. Parente, and J. Santos, "Precise x-ray energies of gadolinium determined by a combined experimental and theoretical approach," *Journal of Quantitative Spectroscopy and Radiative Transfer*, vol. 236, p. 106585, 2019. [Online]. Available: http://www.sciencedirect.com/science/article/pii/S0022407319303863

[7] Y. Ménesguen and M.-C. Lépy, "Efficiency calibration and surface mapping of an energy-dispersive detector with SOLEX: A compact tunable monochromatic x-ray source," *Nuclear Instruments & Methods In Physics Research A*, vol. 695, pp. 193–196, 2012.

[8] S. T. Perkins, "Tables and graphs of atomic subshell and relaxation data derived from the LLNL Evaluated Atomic Data Library (EADL) Z = 1-100," Lawrence Livermore National Laboratory, UCRL-50400 30, 1991.

[9] S. Puri, D. Mehta, B. Chand, and P. N. Trehan, "L Shell Fluorescence Yields and Coster-Kronig Transition Probabilities for the Elements with $25 \leq Z \leq 96$," *X-ray Spectrometry*, vol. 22, pp. 358–361, 1993.

[10] M. O. Krause, "Atomic Radiative and Radiationless Yields for K and L Shells," *Journal of Physical and Chemical Reference Data*, vol. 8, no. 2, pp. 307–328, 1979.

[11] J. L. Campbell, "Fluorescence yields and Coster-Kronig probabilities for the atomic L subshells," *Atomic Data and Nuclear Data Tables*, vol. 85, pp. 291–315, 2003.

[12] T. Schoonjans, A. Brunetti, B. Golosio, M. Sanchez del Rio, V. Solé, C. Ferrero, and L. Vincze, "The xraylib library for X-ray–matter interactions. Recent developments," *Spectrochim. Acta B*, vol. 66, no. 11-12, pp. 776–784, 2011.

[13] Y. Ménesguen, M. Gerlach, B. Pollakowski, R. Unterumsberger, M. Haschke, B. Beckhoff, and M.-C. Lépy, "High accuracy experimental determination of copper and zinc mass attenuation coefficients in the 100 eV to 30 keV photon energy range," *Metrologia*, vol. 53, pp. 7–17, 2016.

[14] J. Sherman, "The theoretical derivation of fluorescent X-ray intensities from mixtures," *Spectrochimica Acta*, vol. 7, pp. 283–306, 1955.

[15] D. E. Cullen, J. H. Hubbell, and L. Kissel, "EPDL97: the Evaluated Photon Data Library, '97 Version"," *UCRL-50400*, vol. 6, no. 5, 1997, consultation date: 2017. [Online]. Available: https://www-nds.iaea.org/epdl97/document/epdl97.pdf

[16] H. Ruellan, M.-C. Lépy, M. Etcheverry, J. Plagnard, and J. Morel, "A new spectra processing code applied to the analysis of ^{235}U and ^{238}U in the 60-200kev energy range," *Nuclear Instruments & Methods In Physics Research A*, vol. 369, pp. 651–656, 1996.

[17] J. L. Campbell and T. Papp, "Widths of atomic K-N7 levels," *Atomic Data and Nuclear Data Tables*, vol. 77, pp. 1–56, 2001.

[18] J. H. Scofield, "Relativistic Hartree-Slater values for K and L X-ray emission rates," *Atomic Data and Nuclear Data Tables*, vol. 14, pp. 121–137, 1974.

[19] JCGM, *Evaluation of measurement data - Guide to the expression of uncertainty in measurement*. BIPM, 2008, consultation date: 2015. [Online]. Available: http://www.bipm.org/fr/publications/guides/gum.html

[20] S. Singh, D. Mehta, R. R. Garg, S. Kumar, M. L. Garg, N. Singh, P. C. Mangal, J. H. Hubbell, and P. N. Trehan, "Average L-Shell Fluorescence Yields for Elements $56 \leq Z \leq 92$," *Nuclear Instruments and Methods B*, vol. 51, pp. 5–10, 1990.

[21] T. Papp, J. L. Campbell, and S. Raman, "Fluorescence and Coster-Kronig yields of the L1 shell in gadolinium," *Physical Review A*, vol. 58, p. 3537, 1998.